An Efficient Model for Robust Load Frequency Control in Multi-Area Power Systems with Communication Delays

Li Jin[a,b,c,d], Yong He[a,b,c,*], Chuan-Ke Zhang[a,b,c], Xing-Chen Shangguan[a,b,c,d], Lin Jiang[d], Min Wu[a,b,c]

[a]School of Automation, China University of Geosciences, Wuhan 430074, China
[b]Hubei Key Laboratory of Advanced Control and Intelligent Automation for Complex Systems, Wuhan 430074, China
[c]Engineering Research Center of Intelligent Technology for Geo-Exploration, Ministry of Education, Wuhan 430074, China
[d]Department of Electrical Engineering and Electronics, University of Liverpool, Liverpool L69 3GJ, United Kingdom

Abstract

This paper proposes an effective method such that the robust load frequency control (LFC) scheme can be designed efficiently for the large-scale power system with time delay. A novel constraint time-delayed ordinary differential equation (CTODE) model is proposed, based on which a new bounded real lemma (BRL) is established for the H_∞ performance analysis. The CTODE model is investigated considering the small number of remote signals influenced by delays in the LFC scheme. It consists of three parts, i.e., a delayed part includes the remote states, whose order is far less than that of the original system and remains unchanged with the increased scale of the power system, and a delay-free (related) part involves the local signals irrelevant (subjected) to the delayed states. Then, the BRL is established by constructing a new Lyapunov functional where the delayed part is employed to address the delay information. Case studies are implemented on the three-area LFC scheme and 39 bus New England systems. Compared with the existing methods, the developed BRL is available for the stability analysis with minor conservatism, but the calculation complexity is greatly reduced in large-scale power systems. Moreover, based on the CTODE model and original model, the robust controllers are designed and compared in robustness against load variations, time delays, and parameter uncertainties. Similar dynamic performance is verified for these two kinds of controllers through robust performance analysis, system eigenvalue analysis, and simulation studies.

Keywords: Load frequency control, CTODE model, time delay, delay-dependent robust method.

1. Introduction

Load frequency control (LFC) aims to maintain the frequency of power systems at scheduled values [1, 2]. The LFC scheme requires the measurement signals of frequency deviation and tie-line power change. Then, the control input can be formed and transformed to the power plant to eliminate the frequency deviation. The communication channels are deployed to transmit this information, inducing time delays inevitably [3, 4, 5]. These time delays influence the safe operation of the LFC schemes [6, 7]. The frequency-domain direct method and time-domain indirect method are reported to evaluate the influence of such time delays on the system frequency stability [8]. The former can deal with the constant delays and obtain the accurate delay margins [9]. The latter is preferred to calculate the approximate delay margins for the power system with random and time-varying delays [10]. For instance, based on the Lyapunov theory, delay-dependent criteria are presented in terms of the linear matrix inequalities (LMIs) to calculate the delay margins of the delayed LFC system [11, 12]. For the H_∞ performance analysis, the bounded real lemma (BRL) is established to design the robust controllers, which decreases the influence of external disturbance on the system frequency stability [13]. Moreover, some probabilistic information of time delays is considered in the derived condition for designing a robust LFC system [14]. Under a preset delay upper bound, the robust performance of the designed LFC controller is optimized by minimizing the H_∞ index in the BRL [15]. Such controllers enable the frequency stability of the power system with any delays less than the preset upper bound.

However, before all those analysis/ synthesis methods can be applied to the real-world power systems, the heavy computational burden of the time-domain LMI based methods remains to be concerned. The solvers provided by the Matlab toolbox have limited capability of solving large-scale LMIs. Thus, existing researches attempt to improve the calculation efficiency by decreasing the order of the derived LMIs together with the number of decision variables [16, 17, 18]. Note that the authors of [16] focus on the obtained LMI condition without considering the special features of the LFC scheme. The reconstructed methods are proposed in [17, 18] by investigating the sparse characteristic of the LFC model. The original model is divided into the delayed part and the delay-free part while containing

☆This work is supported by the National Natural Science Foundation of China under Grants 61973284, 62022074, and 61873347, the Hubei Provincial Natural Science Foundation of China under Grants 2019CFA040, the 111 Project under Grant B17040, and the Fundamental Research Funds for National Universities, China University of Geosciences (Wuhan).

*Corresponding author
Email address: heyong08@cug.edu.cn (Yong He)

the delay information in the delayed part. However, these methods cannot be extended for controller design since they require to explore the zero elements of coefficient matrices with known controller gains. Even though the reconstructed model [19] is reported to be available for controller design, its delayed part has the increased order with the large-scale LFC system. Thus, the existing reconstructed models are unavailable for the controller design in large-scale power systems.

In addition, model order reduction represents a common procedure to decrease the complexity of tuning controllers in large-scale power systems [20, 21]. Coherency-based approaches have been reported to obtain the reduced-order models for large power systems [22, 23]. As the nature of coherency properties varies as operating conditions change, it is challenging to realize reduced-order models accurately by deploying the coherency-based techniques. The balanced truncation is employed to find a reduced-order model of the entire power system by computing a subspace of the product of the observability and controllability gramians [24, 25]. To further reduce the time required by the balanced truncation-based method, a reduced-order model of the entire system is computed using the cross-gramian approach [26, 27]. The cross-gramian is calculated by resolving the Sylvester equation [28]. Note that these techniques are not specially developed for the multi-area LFC scheme. Moreover, they are generally studied for the entire power system, ignoring the physical meaning of each individual state and its participation into the LFC scheme. Additionally, the reduced-order models just exhibit approximation to the dynamic of the original models while not retaining all characteristics. Although the controllers are designed efficiently by using the reduced-order models, their dynamic performance is degraded in comparison with those based on the original model.

This paper investigates a novel method to obtain the PI-based robust controller in the large-scale LFC power system efficiently. A constraint time-delayed ordinary differential equation (CTODE) model is proposed, and a new BRL is established for the H_∞ performance analysis. The CTODE model has three parts, i.e., the delayed part consists of the remote signals, including the frequency deviation and tie-line power change, whose dynamic is described as the ordinary differential equation (ODE); the local signals are decomposed into the delay-free part (expressed as the delay-free ODE) and the delay-related part (described by the time-delayed ordinary differential equation (TODE)). Note that the CTODE model is an equivalent form of the original model, differing from the reduced-order models [20]-[28] with system information missed. To obtain the CTODE model, the participation of each state into the LFC model is investigated instead of exploring the feature of the coefficient matrices. When the controller remains to be resolved, the CTODE model is still realizable while the previous models [17, 18] lose availability. Moreover, the information of time delay is comprised in the ODE, whose dimension keeps unchanged with the increased scale of the power system. In contrast, the order of the delayed part is increased in the reconstructed model [19]. Then, based on the CTODE model, a new Lyapunov functional is constructed whose integral terms employ the delayed part to deal with the time delay. Hence, a delay-dependent criterion is established, and it is eligible for designing robust controllers in a large power system while the methods in [17, 18, 19] are ineffective. Case studies are completed on the three-area LFC scheme and 39 bus New England (NE39) systems. Compared with the previous approaches, the proposed method is validated to have obviously improved calculation efficiency. For given controllers, the proposed method is eligible for the delay-dependent stability analysis without considering disturbance, and the delay margins are calculated with the minor cost of accuracy. To verify the effectiveness of the controllers designed based on the CTODE model, the controllers obtained on the original model are also shown. These two kinds of controllers are tested on the original system, respectively. Based on the robust performance analysis, system eigenvalue analysis, and simulation studies, they have been verified with the similar dynamic performances in terms of robustness against time delays, load variations, and parameter uncertainties.

The remainder of this paper is organized as follows. Section 2 shows the dynamic model of the multi-area LFC scheme and a new CTODE model. Section 3 constructs a new Lyapunov functional based on the CTODE model and a robust method is presented. Section 4 adopts the three-area LFC scheme and NE39 systems to demonstrate the effectiveness of the proposed method. Conclusions are given in Section 5.

2. Multi-Area LFC Scheme

The dynamic model is shown for the multi-area LFC scheme with time delays. A new model is then proposed, based on which a new BRL is presented for the H_∞ performance analysis. Then, the H_∞ controllers can be obtained effectively and efficiently for large-scale LFC schemes.

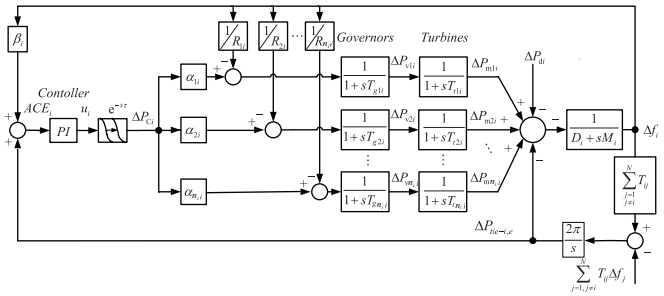

Figure 1: Structure of control area i in the multi-area LFC scheme.

2.1. Dynamic Model of Multi-Area LFC Scheme

In the multi-area LFC system, the structure of area i is depicted in Figure 1 where n_i generators are equipped and installed with non-reheat turbines; exponential block $e^{-s\tau}$ shows the delays arising in the communication channels; $\Delta f_i, \Delta P_{tie-i,e}, \Delta P_{mn_i i}$, $\Delta P_{vn_i i}$ are the deviation of frequency, tie-line power exchange, mechanical output of generator, and valve position, respectively; $M_i, D_i, T_{gn_i i}, T_{tn_i i}$, $R_{n_i i}$ are the moment of inertia of generator unit, generator unit damping coefficient, time constant of the governor, time constant of the turbine

Table 1: List of abbreviations

LFC	load frequency control
LMIs	linear matrix inequalities
CTODE	constraint time-delayed ordinary differential equation
TODE	time-delayed ordinary differential equation
ODE	ordinary differential equation
NE39	39 bus New England
ACE	area control error
RPI	robust performance index
PSO	particle swarm optimization
GRC	generation rate constraints
GDB	governor dead band
PV	parameter variation
ITAE	integral of the time multiplied absolute value of the error
FD	figure of demerit

and speed drop, respectively, and β_i, $\alpha_{n_i i}$ are the frequency bias factor of area i and ramp rate factor, respectively.

The area control error (ACE) signal for area i is defined as

$$ACE_i = \beta_i \Delta f_i + \Delta P_{tie-i,e}. \tag{1}$$

Similar to [13], a PI-type LFC controller is potentially chosen for the LFC scheme. That is,

$$u_i(t) = -K_{Pi} ACE_i(t) - K_{Ii} \int ACE_i(t)dt \tag{2}$$

where K_{Pi} and K_{Ii} are proportional and integral gains, respectively.

Assume the equal time delays appearing in all control areas and satisfying $0 \le \tau(t) \le h$ and $\dot{\tau}(t) \le \mu$.

For the multi-area LFC scheme composed by N control areas, it can be described by the following TODE:

$$\begin{cases} \dot{x}(t) = Ax(t) + BKCx(t-\tau(t)) + F\omega(t) \\ y(t) = Cx(t) \end{cases} \tag{3}$$

where

$$\begin{aligned}
x(t) =& [\tilde{x}_1(t),\ \tilde{x}_2(t),\ \ldots,\ \tilde{x}_N(t)]^T \\
y(t) =& [y_1(t),\ y_2(t),\ \ldots,\ y_N(t)]^T \\
\omega(t) =& [\Delta P_{\mathrm{d}1}(t),\ \Delta P_{\mathrm{d}2}(t),\ \ldots,\ \Delta P_{\mathrm{d}N}(t)]^T \\
\tilde{x}_i(t) =& \left[\Delta f_i, \Delta P_{tie-i,e}, \Delta P_{m1i}, \ldots, \Delta P_{mn_i i}, \Delta P_{v1i}, \ldots, \Delta P_{vn_i i}, \int ACE_i\right]^T \\
y_i(t) =& \left[ACE_i(t),\ \int ACE_i(t)\right]^T
\end{aligned}$$

with

$$\begin{aligned}
A &= \begin{bmatrix} A_{11a} & \ldots & A_{1Na} \\ \vdots & \ddots & \vdots \\ A_{N1a} & \ldots & A_{NNa} \end{bmatrix} \\
B &= \mathrm{diag}\{B_1,\ B_2,\ \ldots,\ B_N\} \\
C &= \mathrm{diag}\{C_1,\ C_2\ \ldots\ C_N\} \\
F &= \mathrm{diag}\{F_1,\ F_2,\ \ldots,\ F_N\} \\
K &= \mathrm{diag}\{K_1,\ K_2,\ \ldots,\ K_N\} \\
K_i &= [K_{Pi}\ K_{Ii}]
\end{aligned}$$

$$\begin{aligned}
A_{ii} &= \begin{bmatrix} \tilde{A}_i & 0 \\ \tilde{C}_i & 0 \end{bmatrix},\ A_{ij} = \begin{bmatrix} \tilde{A}_{ij} & 0 \\ 0_{1\times(2n_i+2)} & 0 \end{bmatrix},\ B_i = \begin{bmatrix} \tilde{B}_i \\ 0 \end{bmatrix} \\
C_i &= \begin{bmatrix} \tilde{C}_i & 0 \\ 0_{1\times(2n_i+2)} & 1 \end{bmatrix},\ F_i = \begin{bmatrix} -\frac{1}{M_i} \\ 0_{(2n_i+2)\times 1} \end{bmatrix} \\
\tilde{A}_i &= \begin{bmatrix} A_{11i} & A_{12i} & 0_{2\times n_i} \\ 0_{n_i\times 2} & A_{22i} & A_{23i} \\ A_{31i} & 0_{n_i\times n_i} & A_{33i} \end{bmatrix}, \tilde{A}_{ij} = \begin{bmatrix} 0 & 0 & 0_{1\times 2n_i} \\ -2\pi T_{ij} & 0 & 0_{1\times 2n_i} \\ 0_{2n_i\times 1} & 0_{2n_i\times 1} & 0_{2n_i\times 2n_i} \end{bmatrix} \\
A_{11i} &= \begin{bmatrix} -\frac{D_i}{M_i} & -\frac{1}{M_i} \\ 2\pi \sum_{j=1, j\neq i}^{N} T_{ij} & 0 \end{bmatrix}, A_{12i} = \begin{bmatrix} \frac{1}{M_i} & \cdots & \frac{1}{M_i} \\ 0 & \cdots & 0 \end{bmatrix} \\
A_{22i} &= -A_{23i} = -\mathrm{diag}\left\{\frac{1}{T_{t1i}}, \cdots, \frac{1}{T_{tn_i i}}\right\} \\
A_{31i} &= -\begin{bmatrix} \frac{1}{R_{1i}T_{t1i}} & \cdots & \frac{1}{R_{n_i i}T_{tn_i i}} \\ 0 & \cdots & 0 \end{bmatrix}^T,\ \tilde{B}_i = \begin{bmatrix} 0_{2\times 1} \\ 0_{n_i\times 1} \\ B_{3i} \end{bmatrix} \\
A_{33i} &= -\mathrm{diag}\left\{\frac{1}{T_{g1i}}, \cdots, \frac{1}{T_{gn_i i}}\right\},\ B_{3i} = \left[\frac{\alpha_{1i}}{T_{g1i}}, \cdots, \frac{\alpha_{n_i i}}{T_{gn_i i}}\right]^T, \\
\tilde{C}_i &= [\ \beta_i, 1, 0_{1\times 2n_i}\ ],\ \beta_i = \sum_{j=1}^{n_i} \frac{1}{R_{ji}} + D_i.
\end{aligned}$$

Note that considering the multi-area LFC scheme, the tie-line power exchange between each control area satisfies the following equation:

$$\sum_{i=1}^{N} P_{tie-i,e} = 0 \tag{4}$$

Thus, based on (4), state $P_{tie-i,e}$ of (3) can be represented by other state variables so as to reduce the order of system (3) by one, i.e., the order of $x(t)$ is $m = 2\sum_{i=1}^{N} n_i + 3N - 1$.

2.2. A Novel CTODE Model

As can be seen from Figure 1, the ith area obtains remote measurement signals $\Delta f_i(t)$ and $\Delta P_{tie-i,e}(t)$ such that the control centre can formulates control signal u_i to generators. The transmission of these three signals requires communication channels where time delay $\tau(t)$ is induced. Therefore, the delayed states form $u_i(t-\tau(t))$.

Then, the inputs of the governors are affected by the delayed states such that the states of governors can be called delay-related states, i.e.,

$$\Delta \dot{P}_{vi}(t) = f_i\left(u_i(t-\tau(t)), \Delta f_i(t), \Delta P_{vi}(t)\right), i = 1, 2, \ldots, N \tag{5}$$

where function $f_i(\cdot)$ is a proper function, and $\Delta P_{vi}(t) = [P_{v1i}(t), P_{v2i}(t), \ldots, P_{vn_i i}(t)]$.

The inputs of local turbines are only subjected to the outputs of the local governors. Thus, the states employed for the turbines are free to time delays and delayed states, whose formula can be expressed as

$$\Delta \dot{P}_{mi}(t) = g_i\left(\Delta P_{mi}(t), \Delta P_{vi}(t)\right), i = 1, 2, \ldots, N \tag{6}$$

where function $g_i(\cdot)$ is an appropriate function, and $\Delta P_{mi}(t) = [P_{m1i}(t), P_{m2i}(t), \ldots, P_{mn_i i}(t)]$.

Thus, the system state vector $x \in R^m$ can be decomposed into three parts. By re-ranking the states in x, original model (3) can be rewritten as the following TODEs:

$$\dot{x}_1(t) = \chi\left(x_1(t), x_2(t), x_3(t), \omega(t)\right) \tag{7a}$$

$$\dot{x}_2(t) = f\left(x_1(t), x_2(t), x_3(t)\right) \tag{7b}$$

$$\dot{x}_3(t) = g\left(x_1(t), x_2(t), x_3(t), x_1(t-\tau(t))\right) \tag{7c}$$

where $\chi(\cdot)$ is a proper function, $x_1 \in R^{q_1}$ is the delayed vector $x_1(t) = \Big[\Delta f_1(t), \Delta P_{tie-1,e}(t), \int ACE_1(t), \ldots, \Delta f_N(t), \Delta P_{tie-N,e}(t), \int ACE_N(t)\Big]^T$, $x_2 \in R^{q_2}$ denotes the delay-free vector $x_2(t) = [\Delta P_{m1}(t), \ldots, \Delta P_{mN}(t)]$, and $x_3 \in R^{q_3}$ represents the delay-related vector $x_3(t) = [\Delta P_{v1}(t), \ldots, \Delta P_{vN}(t)]$.

Equation (7c) can describe the dynamics of the delayed LFC loop, but it is subject to both the dynamic manifolds of equations (7a) and (7b). Therefore, by regarding ODEs (7a) and (7b) as the constraints of TODE (7c), equation (7) is called the CTODE model, which is illustrated in Figure 2.

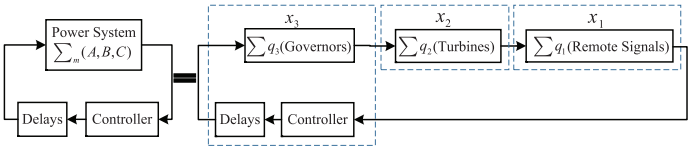

Figure 2: Demonstration of the CTODE model.

It is convenient for us to obtain $\left[x_1^T(t), x_2^T(t), x_3^T(t)\right]^T = Ex(t)$ via an elementary row transformation matrix E, and

$$\begin{cases} \dot{x}_1(t) = A_{11}x_1(t) + A_{12}x_2(t) + A_{13}x_3(t) + F_t\omega(t) \\ \dot{x}_2(t) = A_{21}x_1(t) + A_{22}x_2(t) + A_{23}x_3(t) \\ \dot{x}_3(t) = A_{31}x_1(t) + A_{32}x_2(t) + A_{33}x_3(t) + B_tKC_tx_1(t-\tau(t)) \end{cases} \tag{8}$$

with

$$EAE^{-1} = \begin{bmatrix} A_{11} & A_{12} & A_{13} \\ A_{21} & A_{22} & A_{23} \\ A_{31} & A_{32} & A_{33} \end{bmatrix}, EB = \begin{bmatrix} 0 \\ 0 \\ B_t \end{bmatrix}, CE^{-1} = \begin{bmatrix} C_t^T \\ 0 \\ 0 \end{bmatrix}^T, EF = \begin{bmatrix} F_t \\ 0 \\ 0 \end{bmatrix}$$

To achieve (8) conveniently, transformation matrix E can be selected as the combination of unit vectors. For the multi-area LFC scheme ($N \geq 3$), matrix E is shown in below.

$$E = [E_{N\mathrm{a}}, E_{N\mathrm{b}}, E_{N\mathrm{c}}]^T \tag{9}$$

$$\begin{aligned} E_{N\mathrm{a}} &= [E_1, E_2, E_{2n_1+3}, E_{2n_1+4}, E_{2n_1+5}, E_{2n_1+2n_2+6}, \ldots, \\ &\quad E_{m-2(n_N+n_{N-1})-4}, E_{m-2(n_N+n_{N-1})-3}, E_{m-2n_N-2}, E_{m-2n_N-1}, E_m] \\ E_{N\mathrm{b}} &= [E_3, \ldots, E_{n_1+2}, E_{2n_1+6}, \ldots, E_{2n_1+n_2+5}, \ldots, E_{m-2n_N}, \\ &\quad \ldots, E_{m-2(n_N+n_{N-1})-2}, \ldots, E_{m-2n_N-n_{N-1}-3}, E_{m-n_N-1}] \\ E_{N\mathrm{c}} &= [E_{n_1+3}, \ldots, E_{2n_1+2}, E_{2n_1+n_2+6}, \ldots, E_{2n_1+2n_2+5}, \ldots, E_{m-n_N}, \\ &\quad \ldots, E_{m-2n_N-n_{N-1}-2}, \ldots, E_{m-2n_N-3}, E_{m-1}] \\ E_k &= [0_{1\times(k-1)}, 1, 0_{1\times(m-k)}]^T, k = 1, 2, \ldots, m. \end{aligned}$$

In model (8), the states regarding remote signals are included in delayed vector x_1. The local states are decomposed into delay-free vector x_2 and delay-related vector x_3 since x_2 is no longer subjected to $x_1(t-\tau(t))$ while x_3 is related to $x_1(t-\tau(t))$, The TODE in (8) contains the controllers to be designed. The development of the CTODE model fully concerns the physical meaning of each individual state and its participation into the delayed LFC schemes. Its realization avoids the exploration of the sparse feature of coefficient matrices of the original model together with their non-zero elements required by the reconstructed methods in [17] and [18]. Therefore, the proposed CTODE model is effective when the controller remains to be designed for the LFC system. It shortens the research gap that the reconstructed models [17, 18] become ineffective with unknown controller gains and coefficient matrices.

Note that the proposed model (8) equivalently transforms the original model (3) without losing any system information. Thus, based on the equivalent model, it is expected to design controllers with the almost unreduced dynamic performance, which is superior to the reduced-order models [20]-[28]. The CTODE model contains the time delay in the delayed part $x_1 \in R^{q_1}$. When the Lyapunov functional is constructed to establish a delay-dependent criterion, its delay-related integral terms employ $x_1 \in R^{q_1}$ instead of $x \in R^m$. Due to $q_1 \ll m$, the dimension of the derived criterion can be highly reduced by using the CTODE model. Most importantly, in (8), q_1 remains unchanged with respect to the scale of the concerned system, which prompts the derived criterion to design controllers in large-scale power systems efficiently. Whereas, the reconstructed model presented in [19] contains the delayed part, whose order is increased with the expansion of power systems, limiting its application to a real-world power system.

2.3. Objective

This paper aims to propose an effective method such that the robust LFC scheme in the large power system with time delay can be designed efficiently. A new CTODE model is presented, based on which a new BRL is established for the H_∞ performance analysis. Meanwhile, it can guarantee the stability of the closed-loop system undergoing disturbance and any time delays smaller than the preset upper bounds. A robust method is presented and assures:

1) Under the zero initial state condition, for any nonzero $\omega(t) \in \mathcal{L}_2[0, \infty)$ and a prescribed $\gamma > 0$, inequality $\|y(t)\|_2 \leq \gamma\|\omega(t)\|_2$ holds.
2) System (8) is asymptotically stable considering $\omega(t) = 0$.

Here, a robust performance index (RPI) is defined as $\gamma_{\min} = \min\{\|y\|_2/\|\omega\|_2\}$ to minimize the effect of disturbance $\omega(t)$ on output $y(t)$.

3. Delay-Dependent Robust Method

Based on the CTODE model, a new BRL is given to guarantee that the multi-area delayed LFC scheme is asymptotically stable with a dynamic performance H_∞ index. This condition can guide the design of the desired robust controller.

3.1. H_∞ Performance Analysis

Based on the CTODE model, a newly presented Lyapunov functional is shown in below.

$$V(t) = \xi^T(t)P\xi(t) + \int_{t-\tau(t)}^{t} x_1^T(s)Q_1x_1(s)ds + \int_{t-h}^{t} x_1^T(s)Q_2x_1(s)ds + h\int_{-h}^{0}\int_{t+\theta}^{t} \dot{x}_1^T(s)R\dot{x}_1(s)dsd\theta \quad (10)$$

where $\xi^T(t) = \left[x_1^T(t), x_2^T(t), x_3^T(t), \int_{t-h}^{t} x_1^T(s)ds\right]$, and $P \in R^{(m+q_1)\times(m+q_1)}$, $Q_1, Q_2, R \in R^{q_1\times q_1}$ are matrices to be determined.

Then, the following BRL can be developed, which shows the relationship between the time delay and the H_∞ performance index.

Theorem 1. *For the delay upper bound h, the delay variation upper bound μ, the H_∞ performance index γ, and the controller gain K, system (8) is asymptotically stable and $\sup_{\omega\neq 0} \|y\|_2/\|\omega\|_2 < \gamma$ for any delays satisfying $0 \le \tau(t) \le h$ and $\dot{\tau}(t) \le \mu$, if there exist matrices $P > 0, Q_1 > 0, Q_2 > 0, R > 0$, such that the following LMI holds*

$$\Pi_1 + \Pi_2 < 0 \quad (11)$$

where

$$\begin{aligned}
\Pi_1 &= E_a^T PE_b + E_b^T PE_a + e_1^T(Q_1+Q_2)e_1 - (1-\mu)e_2^T Q_1 e_2 \\
&\quad -e_3^T Q_2 e_3 + h^2 e_{s1}^T R e_{s1} - E_c^T \mathrm{diag}\{R, 3R\} E_c \\
\Pi_2 &= \left[e_1^T\ e_5^T\ e_6^T\right] C_t^T C_t \left[e_1^T\ e_5^T\ e_6^T\right]^T - \gamma^2 e_7^T e_7 \\
E_a &= \left[e_{s1}^T\ e_{s2}^T\ e_{s3}^T\ (e_1-e_3)^T\right]^T \\
E_b &= \left[e_1^T\ e_5^T\ e_6^T\ he_4^T\right]^T \\
E_c &= \left[(e_1-e_3)^T\ (e_1+e_3-2e_4)^T\right]^T \\
e_{s1} &= A_{11}e_1 + A_{12}e_5 + A_{13}e_6 + F_t e_7 \\
e_{s2} &= A_{21}e_1 + A_{22}e_5 + A_{23}e_6 \\
e_{s3} &= A_{31}e_1 + A_{32}e_5 + A_{33}e_6 + B_t K C_t e_2 \\
e_l &= \left[0_{q_1\times(l-1)q_1}, I_{q_1\times q_1}, 0_{q_1\times(4-l)q_1}, 0_{q_1\times q_2}, 0_{q_1\times q_3}, 0_{q_1\times m_\omega}\right] \\
l &= 1,2,3,4 \\
e_5 &= \left[0_{q_2\times 4q_1}, I_{q_2\times q_2}, 0_{q_2\times q_3}, 0_{q_2\times m_\omega}\right] \\
e_6 &= \left[0_{q_3\times 4q_1}, 0_{q_3\times q_2}, I_{q_3\times q_3}, 0_{q_3\times m_\omega}\right] \\
e_7 &= \left[0_{m_\omega\times 4q_1}, 0_{m_\omega\times q_2}, 0_{m_\omega\times q_3}, I_{m_\omega\times m_\omega}\right]
\end{aligned}$$

The proof of Theorem 1 can be found in Appendix II.

Theorem 1 is established based on (8), where the time-varying delay is considered. It can be used to deal with the constant delay by setting $\mu = 0$ and to address the random delay by setting $Q_1 = 0$. Moreover, the investigation of the asymptotical stability concerns the system's internal stability, and it is unnecessary to consider the external disturbance $\omega(t)$. Therefore, Theorem 1 can be turned into the asymptotical stability criterion for system (8) with $\omega(t) = 0$.

As shown in (10), Q_1, Q_2- and R-dependent terms are constructed based on delayed state x_1 to deal with the information of time delay, and the P-dependent augmented term also contains x_1, i.e., the order of x_1 changes the scale of Lyapunov matrices P, Q_1, Q_2 and R, and meanwhile, the decision variables introduced into the LMI of Theorem 1 is affected. Moreover, the order of LMI (11) is $(4q_1 + q_2 + q_3 + m_\omega)$. Therefore, delay state $x_1 \in R^{q_1}$ obviously influences the two key factors that reflect the computation complexity of LMI (11), including the number of decision variables and the maximum order. Many delayed states included in x_1 lead to the high-dimensional of the LMIs with a large number of decision variables. In this paper, the number of delayed states in x_1 is no longer increased with the scale of power systems. It plays a key role in simplifying LMI (11) to improve its calculation efficiency in the large-scale power system.

3.2. Summary of Presented Method

The method proposed in this paper can be summarized in the following steps:

*Step*1. The state-space model of the multi-area LFC system equipped with the PI-type controller is shown in Section 2.1. Based on this model, a new CTODE model is constructed in Section 2.2.

*Step*2. Stability analysis. The presented method can be employed to calculate the delay margins of the three-area LFC scheme with no external disturbance. The YALMIP toolbox and binary search algorithm are used.

*Step*3. Controller design. Based on the proposed method, the controllers are determined efficiently under a preset delay upper bound. The robust dynamics of controllers are optimized by minimizing the H_∞ index.

*Step*4. Robust performance analysis. For the LFC systems equipped with designed controllers, the RPI is calculated with respect to different time delays.

*Step*5. Eigenvalue analysis. The Chebyshev discretization method [12] is deployed to investigate the eigenvalues of the system models with obtained controllers.

*Step*6. Simulation verification. Simulation studies are carried out to verify the effectiveness of the proposed method.

4. Case Studies

Case studies are based on the three-are LFC system and NE39 systems. The scale of the power system is expanded by increasing the number of NE39 system. The information of system parameters for the three-area LFC scheme is shown in Appendix I. Firstly, the proposed method is verified to have enhanced computational efficiency when compared with the previous methods. To achieve fair comparisons, the same calculation environments are used, including a Win 10 PC equipped with an Intel i7 CPU, a 16GB RAM, and a 64-bit operation system. The SDPT3 solver contained in the YALMIP toolbox of MATLAB 2018b is employed to check the feasibility of LMI (11). The required procedures have the same presets. Then, the delay margins are calculated for the three-area LFC system. The BRL established on the CTODE model is verified with a

little conservatism, and it is therefore of practical value to be used in control design. Next, the robust controller design is carried out on the novel CTODE model, and for comparison, the controllers based on the original model are presented. Lastly, by implementing robust performance analysis, system eigenvalue analysis, and simulation verification, the effectiveness of the proposed method is validated.

4.1. Verification of Computational Efficiency Improvement

This part verifies the enhanced calculation efficiency of Theorem 1 (The.1) established on the novel CTODE model by comparing with the delay-dependent criteria based on the reconstructed model [18] (The.re) and the original model (The.or). Numerical verifications are based on three-area LFC schemes with 3,10,20,40,60,80, and 100 generators, i.e., the total number of generators ($n = \sum_{i=1}^{3} n_i$) in the three-area LFC scheme is given. Three computational performance indices are considered, including the maximum order of the Theorem 1 (m_T), the number of decision variables (n_T), and the CPU time in seconds for solver SDPT3 to resolve related problems (t). For The.1, The.re, and The.or, their maximum order is expressed with m_{T1}, m_{T2}, and m_{T3}, respectively; the number of their decision variables are denoted by n_{T1}, n_{T2}, and n_{T3}, respectively, and the required CPU time is t_1, t_2, and t_3, respectively. The following formulas are given to demonstrate these notations:

$$m_{T1} = 3q_1 + m + 3 \tag{12}$$

$$m_{T2} = 3\tilde{q}_1 + m + 3 \tag{13}$$

$$m_{T3} = 3\bar{q}_1 + m + 3 \tag{14}$$

$$n_{T1} = \frac{(m+q_1)(m+q_1+1)}{2} + \frac{3q_1(q_1+1)}{2} \tag{15}$$

$$n_{T2} = \frac{(m+\tilde{q}_1)(m+\tilde{q}_1+1)}{2} + \frac{3\tilde{q}_1(\tilde{q}_1+1)}{2} \tag{16}$$

$$n_{T3} = \frac{(m+\bar{q}_1)(m+\bar{q}_1+1)}{2} + \frac{3\bar{q}_1(\bar{q}_1+1)}{2} \tag{17}$$

where m represents the order of system model, and q_1, $\tilde{q}_1$, and $\bar{q}_1$ denote the number of delayed states required in the CTODE model, reconstructed model, and original model, respectively.

All results are listed in Table 2, where "-" shows that the current calculation environments are unavailable for obtaining the feasible results during limited time range. As can be seen from Table 2, based on the novel CTODE model, q_1 is kept as a constant regardless of the increased scale of the power system. By contrast, considering the original model, $\bar{q}_1$ is always equal to the order of the system model (m), and therefore, it is increased rapidly as more generators are included in each area. Although there is a decrease in $\tilde{q}_1$ for the reconstructed model, the value of $\tilde{q}_1$ still increases as the system order becomes higher.

In order to develop the BRL with less conservatism, we have to make use of the delay information contained in the system model. An appropriate Lyapunov functional is constructed, whose delayed terms deploy the delayed states. From equations (12)-(14), the maximum order of derived criteria linearly increases with respect to the number of delayed states. Mostly, the sharp rise in the delayed states lets the criteria have lots of decision variables due to the square growth as shown in equations (15)-(17). From Table 2, the proposed method based on the CTODE is available even though 100 generators are equipped. In contrast, the reconstructed model is not available for the power system with over 40 generators. As for the original model, its application is limited to the system with no more than 20 generators installed.

Table 2: Comparisons for computational performance of the theorems based on different models

Methods								
	n	3	10	20	40	60	80	100
	m	14	28	48	88	128	168	208
The.1	q_1	8	8	8	8	8	8	8
	m_{T1}	41	55	75	115	155	195	235
	n_{T1}	361	774	1,704	4,764	9,424	15,684	23,544
	t_1 (s)	0.6	2	7	31	156	311	934
The.re [18]	$\tilde{q}_1$	11	18	28	48	68	88	108
	m_{T2}	50	85	135	235	335	435	535
	n_{T2}	523	1,594	4,144	12,844	26,344	44,644	67,744
	t_2 (s)	1.7	12	38	516	–	–	–
The.or	$\bar{q}_1$	14	28	48	88	128	168	208
	m_{T3}	59	115	195	355	515	675	835
	n_{T3}	721	2,814	8,184	27,324	57,664	99,204	151,944
	t_3 (s)	5.9	22	268	–	–	–	–

4.2. Validation on Three-area LFC Scheme

1) Stability Analysis: When considering external disturbance $\omega(t) = 0$, we can extend Theorem 1 to the asymptotical stability criterion. Here, we present some results on delay margins for the three-area LFC scheme with each area containing a generator at first. Thus, we have $N = 3$ and $n_1 = 1, n_2 = 1, n_3 = 1$. The following transformation matrix E_{T1} is used to obtain the CTODE model:

$$E_{\mathrm{T1}} = [E_1, E_2, E_5, E_6, E_7, E_{10}, E_{11}, E_{14}, E_3, E_8, E_{12}, E_4, E_9, E_{13}]$$
$$E_k = [0_{1\times(k-1)}, 1, 0_{1\times(14-k)}]^T, k = 1, 2, \ldots, 14.$$

The same random delay is assumed in each area. As random delays are considered, we set the weighting matrix $Q_1 = 0$ in Theorem 1 to obtain the delay margins when various controller gains are given.

The results based on the proposed CTODE model (h_{ctode}), reconstructed model [18] (h_{re}), and the original model (h_{or}), are shown in Table 3. Moreover, Table 4 is listed to clearly show the degree of conservatism introduced by using the CTODE model or reconstructed model. In this table, two relative ratios δ_1 and δ_2 are defined for the CTODE model and reconstructed model, respectively. They are calculated with respect to different controllers. The grey area represents the increased conservatism.

From this table, the degree of decreased accuracy becomes more obvious as the value of K_P increases. Comparing with the reconstructed model, the increase of conservatism is faster

Table 3: Delay margins of three-area LFC calculated by different approaches with respect to various controller gains

	K_P (h_{ctode})							K_P (h_{re})							K_P (h_{or})						
K_I	0	0.05	0.1	0.15	0.2	0.25	0.3	0	0.05	0.1	0.15	0.2	0.25	0.3	0	0.05	0.1	0.15	0.2	0.25	0.3
0.05	30.8	31.2	30.1	28.9	27.6	26.3	24.9	30.8	31.4	30.7	29.5	28.2	26.9	25.5	30.8	31.4	31.1	30.0	28.7	27.3	25.9
0.10	15.1	15.6	15.5	14.9	14.2	13.6	12.9	15.1	15.6	15.9	15.4	14.8	14.1	13.4	15.1	15.6	16.0	15.7	15.1	14.4	13.7
0.15	9.8	10.2	10.4	10.2	9.8	9.3	8.8	9.8	10.2	10.4	10.6	10.2	9.8	9.3	9.8	10.2	10.4	10.7	10.5	10.1	9.6
0.20	7.2	7.5	7.7	7.8	7.5	7.2	6.8	7.2	7.5	7.7	7.9	7.9	7.6	7.2	7.2	7.5	7.7	7.9	8.0	7.8	7.5
0.25	5.6	5.8	6.0	6.2	6.2	5.9	5.6	5.6	5.8	6.0	6.2	6.3	6.2	6.0	5.6	5.8	6.0	6.2	6.3	6.3	6.1
0.30	4.6	4.7	4.9	5.0	5.1	5.0	4.8	4.6	4.7	4.9	5.0	5.1	5.2	5.1	4.6	4.7	4.9	5.0	5.1	5.2	5.2

Table 4: Comparisons of conservatism introduced by using CTODE model or reconstructed model

	K_P ($\delta_1(\%) = \frac{h_{or}-h_{ctode}}{h_{or}}$)						
K_I	0	0.05	0.1	0.15	0.2	0.25	0.3
0.05	0.0%	0.8%	3.3%	3.6%	3.7%	3.7%	3.8%
0.10	0.0%	0.0%	3.3%	5.4%	5.8%	6.1%	6.3%
0.15	0.0%	0.0%	0.0%	4.9%	6.8%	7.4%	7.7%
0.20	0.0%	0.0%	0.0%	0.8%	6.2%	7.6%	8.3%
0.25	0.0%	0.0%	0.0%	0.0%	2.2%	6.9%	8.2%
0.30	0.0%	0.0%	0.0%	0.0%	0.0%	3.5%	7.3%
	K_P ($\delta_2(\%) = \frac{h_{or}-h_{re}}{h_{or}}$)						
K_I	0	0.05	0.1	0.15	0.2	0.25	0.3
0.05	0.0%	0.0%	1.3%	1.5%	1.6%	1.6%	1.6%
0.10	0.0%	0.0%	0.4%	1.7%	2.1%	2.3%	2.5%
0.15	0.0%	0.0%	0.0%	0.9%	2.2%	2.6%	2.9%
0.20	0.0%	0.0%	0.0%	0.0%	1.7%	2.6%	3.0%
0.25	0.0%	0.0%	0.0%	0.0%	0.0%	2.1%	2.9%
0.30	0.0%	0.0%	0.0%	0.0%	0.0%	0.1%	2.4%

based on the CTODE model. Thus, the grey area for the C-TODE model based criterion is more extensive in comparison with the condition established with the reconstructed model. Whereas, the conservatism introduced by the presented method is less than 9%, which is acceptable due to the significant improvements on the computation efficiency as shown in Section 4.1. Therefore, it can be expected that the proposed method can be used to design controllers in large power systems while guaranteeing their dynamic performances.

2) Controller Design: Assume the random delays are introduced into the three-area LFC scheme. The upper bounds are equal to $2s$, i.e., $h_{\text{given}} = 2s$. In this case, set $Q_1 = 0$ in Theorem 1 where the relationship is shown between γ and the PI gains. To improve the robustness of designed controllers against time delays, load disturbance, and parameter variations, we need to solve the following optimization problem:

Minimize $\gamma_{\min} = \varrho(h_{\text{given}}, K)$

Subject to

$$K = \text{diag}\{[K_{P1}, K_{I1}], [K_{P2}, K_{I2}], [K_{P3}, K_{I3}]\}$$
$$K_{P\min} \le K_{Pi} \le K_{P\max}$$
$$K_{I\min} \le K_{Ii} \le K_{I\max}, i = 1, 2, 3.$$

Various kinds of optimization algorithms can be used to address the above problem. Based on the results in [29], the PSO algorithm is utilized for numerical optimization in this paper. Figure 3 shows the simplified flowchart of the H_∞ based PI gains tuning.

For the step of initialisation, the following parameters should be presented:

- Set position bounds $X_{\min} = -1$ and $X_{\max} = 1$, velocity bounds $V_{\min} = -0.3$ and $V_{\max} = 0.3$, inertia weight bounds $w_{\min} = -0.3$ and $w_{\min} = 0.3$, acceleration constants $c_1 = c_2 = 2$, population size $N_p = 15$, maximal iteration time $\nu_{\max} = 35$, and initial iteration time $\nu = 0$.
- Obtain random position $X_0 \in [X_{\min}, X_{\min}]$ (i.e. N_p sets of gains $K = \text{diag}\{[K_{P1}, K_{I1}], [K_{P2}, K_{I2}], [K_{P3}, K_{I3}]\}$ and velocity $V_0 \in [V_{\min}, V_{\max}]$.
- Set the search interval $[\gamma_{\text{start}}, \gamma_{\text{end}}]$ and compute the fitness.
- Find the best position for each particle, $pBest$, and the best position within all particles, $gBest$ (i.e. set $\varrho(h_{\text{given}}, pBest_j) = \varrho(h_{\text{given}}, X_{0,j}), j = 1, 2, \ldots, N_p$ and $pBest = X_0$, and set $gBest = X_{0,j}, j = 1, 2, \ldots, N_p$ such that $\varrho(h_{\text{given}}, gBest) = \min \varrho(h_{\text{given}}, X_{0,j}), j = 1, 2, \ldots, N_p$.

For the step of updating the velocities and the positions, the following conditions are applied:

$$w(\nu) = w_{\max} - (w_{\max} - w_{\min})/(\nu_{\max}\nu) \tag{18}$$

$$V_{\nu+1} = \begin{cases} V_{\min}, \ V_{\nu+1} < V_{\min} \\ w(\nu)V_\nu + c_1 \cdot \text{ rand } \cdot (pBest - X_\nu) \\ +c_2 \cdot \text{rand} \cdot (gBest - X_\nu), \ V_{\nu+1} \in [V_{\min}, V_{\max}] \\ V_{\max}, \ V_{\nu+1} > V_{\max} \end{cases} \tag{19}$$

$$X_{\nu+1} = \begin{cases} X_{\min}, \ X_{\nu+1} < X_{\min} \\ X_\nu + V_{\nu+1}, \ X_{\nu+1} \in [X_{\min}, X_{\max}] \\ X_{\max}, \ X_{\nu+1} > X_{\max} \end{cases} \tag{20}$$

where X_ν and $X_{\nu+1}$ are positions in the ν^{th} and $(\nu+1)^{\text{th}}$ iterations, respectively; V_ν and $V_{\nu+1}$ are the velocities in the ν^{th} and $(\nu+1)^{\text{th}}$ iterations, respectively; $w(\nu)$ is the inertia weight in the ν^{th} iteration, and rand is a randomly generated between 0 and 1.

Therefore, controller K_1 is listed in Table 5, where controller K_2 for the original model is displayed for comparison. As can be seen from Figure 3, when the controller is optimized through minimizing γ, meanwhile, the feasibility of LMI (11) is checked. If LMI (11) keeps unfeasible with one given controller gain (particle), i.e., $\gamma_{\text{end}} = \gamma_{\text{e0}}$, we will move to the next particle, and the current particle will be removed until we find a feasible particle. Thus, for a given delay upper bound, the final

obtainment of K_1 and K_2 enables the feasibility of LMI (11). From Table 5, controllers K_1 and K_2 are obtained under similar RPI $\gamma_{\min}$. Therefore, controller K_1 is expected to perform as well as controller K_2.

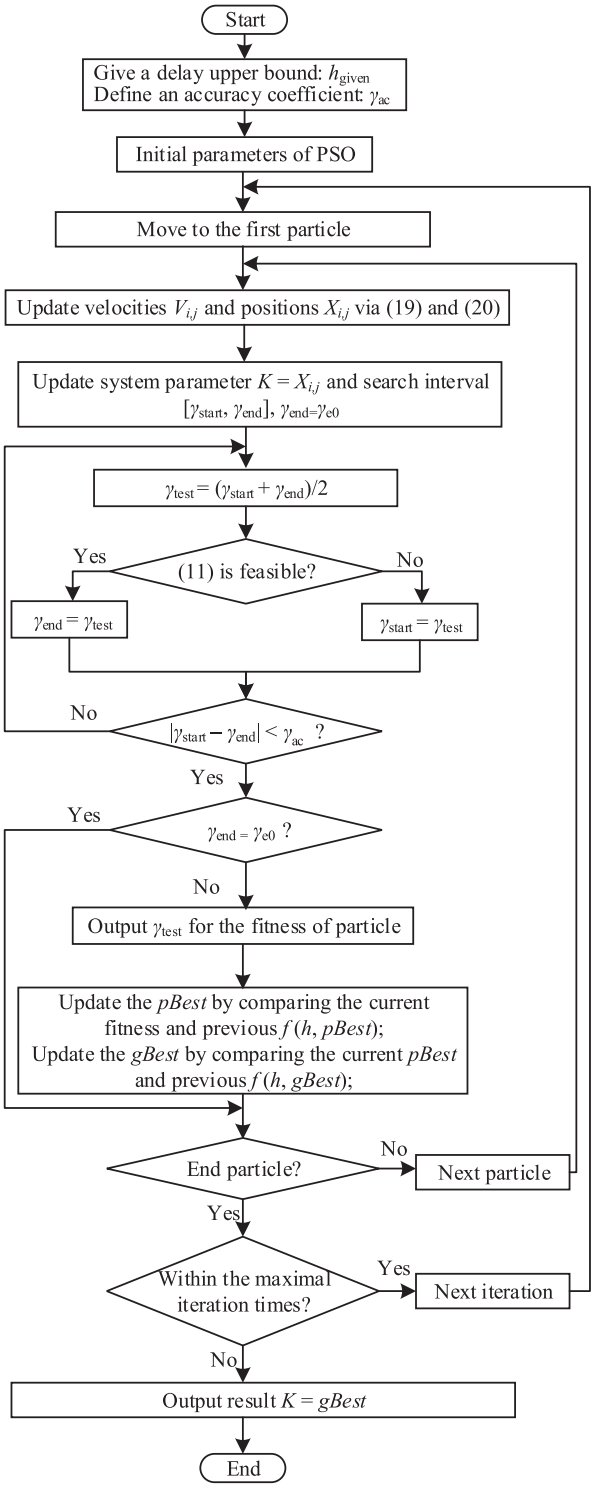

Figure 3: Simplified flowchart for the PSO-based controller gain tuning.

3) Robust Performance Analysis: The minimal H_∞ index is obtained when the closed-loop systems are equipped with controllers K_1 or K_2 and different time delays are induced in the communication networks. The results are depicted in Figure 4. Based on this figure, the RPI $\gamma_{\min}$ is increased with the increased preset of time delays no matter which controller is employed for the LFC system. Controller K_1 performances similarly to controller K_2 due to the same preset of time delay realizing almost identical $\gamma_{\min}$. Moreover, controllers K_1 and K_2 have the same robustness against the time delays as both of them are designed considering $h_{\text{given}} = 2s$, but they can stabilize the LFC scheme with a time delay equal to 5 s. The effectiveness of the proposed method in guaranteeing the robust performance of the obtained controller is verified.

Table 5: Controllers obtained for three-area LFC and NE39 system using C-TODE model and original model

Area	CTODE model		Original model	
	K_1 ($\gamma_{\min}$ = 4.18)	K_3 ($\gamma_{\min}$ = 7.51)	K_2 ($\gamma_{\min}$ = 4.11)	K_4 ($\gamma_{\min}$ = 7.74)
1	-[0.16 0.29]	-[0.46 0.20]	-[0.24 0.30]	-[0.45 0.20]
2	-[0.19 0.28]	-[0.27 0.22]	-[0.20 0.27]	-[0.16 0.25]
3	-[0.19 0.28]	-[0.20 0.22]	-[0.23 0.25]	-[0.04 0.15]

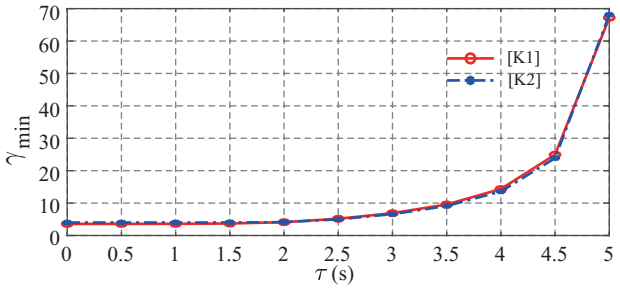

Figure 4: Minimal RPI $\gamma_{\min}$ with respect to various upper bounds h under controllers K_1 and K_2.

4) *System Eigenvalue Analysis:* In this part, the Chebyshev discretization method [31] is utilized to calculate the eigenvalues of the system models equipped with controllers K_1 or K_2. It is reported that selecting 10 Chebyshev points is enough for analyzing [32]. Through the eigenvalue analysis, we aim to show that the controllers designed based on the CTODE model and original model have highly similar robust performance against time delays. Moreover, as the delay upper bound increases, the LFC systems equipped with these two different controllers have almost same eigenvalues loci, which demonstrates the effectiveness of the proposed controller K_1 in dynamic behaviors.

Firstly, set the upper bound of time delay as 5 s, the eigenvalues calculated for the three-area LFC scheme are shown in Figure 5(i). As we can see, even though controllers K_1 and K_2 are designed under $h_{\text{given}} = 2s$, they totally enable the LFC schemes to be stable due to all system eigenvalues lying on the left side. Also, the locations of eigenvalues obtained from the LFC system modeled with controller K_1 are closed to that of eigenvalues developed for the model with controller K_2, respectively. It is verified that controllers K_1 and K_2 have similar robustness against time delays.

Secondly, the case that delay margins increase from 500 ms to 5 s with the step of 500 ms is taken into account. Fig-

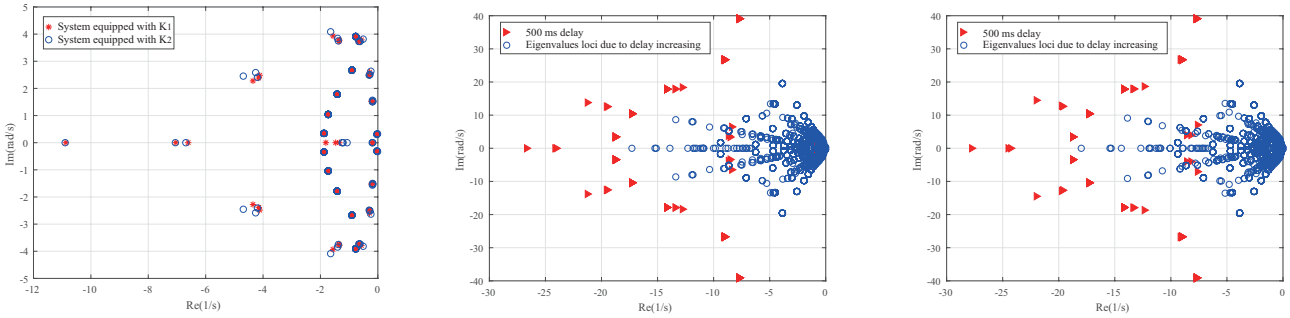

(i) (ii) (iii)

Figure 5: (i) Eigenvalues of three-area LFC scheme equipped with K_1 or K_2. (ii) Eigenvalues loci of three-area LFC scheme equipped with K_1 as delay increases. (iii) Eigenvalues loci of three-area LFC scheme equipped with K_2 as delay increases.

ure 5(ii) and 5(iii) display the eigenvalues' location variations of the LFC systems controlled by K_1 or K_2, respectively. With the increase of time delays, there exist apparent right shifts for the locations of eigenvalue, and their similar tendencies can be observed from these two figures. Therefore, these numerical results show that dynamic performance of controllers K_1 and K_2 behaves similarly in terms of robustness against different time delays.

5) Simulation Verification: For simulation, the generation rate constraints (GRC) and governor dead band (GDB) are two typical nonlinearities in the actual power system, which should be taken into account [30]. GDB is defined as the total magnitude of a sustained speed change, within which there is no resulting change in valve position. It is depicted in the left-hand block of Figure 6. GRC is caused by the limitation of thermal and mechanical movements. The right-hand block of Figure 6 describes the GRC, where V_v and V_l are the maximum and minimum limits that restrict the rate of valve (gate) closing (opening) speeds, respectively. Here, the GRC is set as ±0.1 pu/min, and the range of GDB is given as 0.036 HZ [6].

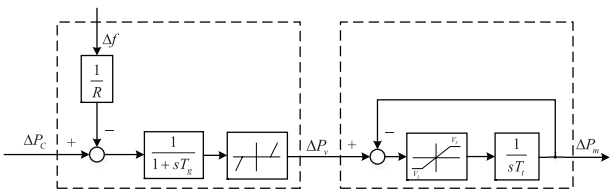

Figure 6: Structures of GRC and GDB in the LFC scheme.

The closed-loop systems equipped with controllers K_1 and K_2 are tested in the presence of step or random changes of load disturbances and time delays, respectively. It is verified that based on the proposed CTODE model, the dynamic performance of K_1 is not reduced in comparison with K_2 obtained with the original model. Moreover, by taking the step disturbances and step (random) time delays into account, the dynamic behaviors of controller [C_1] presented in [4] are also compared with those of controllers K_1 and K_2, including frequency deviation, tie-line power flow, etc. Hence, we can show that the method proposed can be used to design better controllers than the existing method does.

Considering the following scenarios , the random load fluctuations ($\Delta P_{d1}, \Delta P_{d2}, \Delta P_{d3} \in [-0.02, 0.02]$ pu) and time delays ($\tau(t) \in [0, 10]$ s) that are assumed to be applied to the three-area LFC system, are given in Figure 7 (a) and Figure 7 (b), respectively. The ACE and control signals of the LFC are updated every 2 s. The maximum upper bound of the random delay is equivalent to the five sampling steps delay in the controller loop (bigger than the preset delay upper bound $\tau_{\text{given}} = 2$s). It aims to show the robustness of the designed controller against time delays.

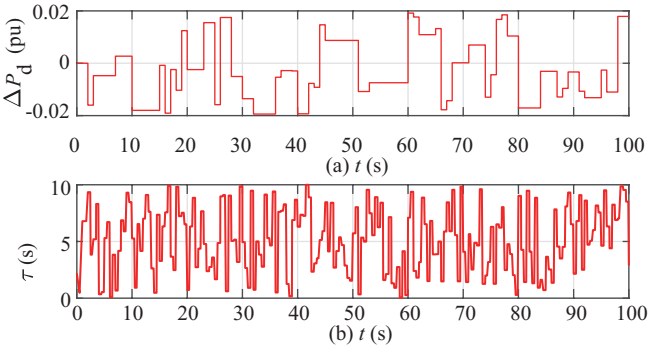

Figure 7: (a) random load change. (b) random time delay

For scenario 1, the step fluctuations are applied to the three-area LFC systems, i.e., $\Delta P_{d1} = 0.1$ pu, $\Delta P_{d2} = 0.08$ pu,$\Delta P_{d3} = 0.05$ pu. Firstly, the constant time delays are set as 4 s, and the responses of areas 1 are given in Figure 8. Here, as the responses of areas 1, 2 and, 3 are similar, only the responses of area 1 are recorded. Secondly, the random delay in Figure 7 (b) is assumed in each area. Figure 9 reveals the responses of the first area. It is concluded that the dynamic performances of controller K_1 obtained from the proposed method are almost unreduced compared with those of K_2 in terms of the robustness against external disturbance and time delays. In addition, both K_1 and K_2 enable the LFC system to have smaller frequency derivation and tie-line power changes than C_1 does, which shows the improved performance of the proposed method in this paper.

For scenario 2, both the random load fluctuations and time delays shown in Figure 7 are assumed to be applied to three areas. Three types of system responses are recorded in Figure 10.

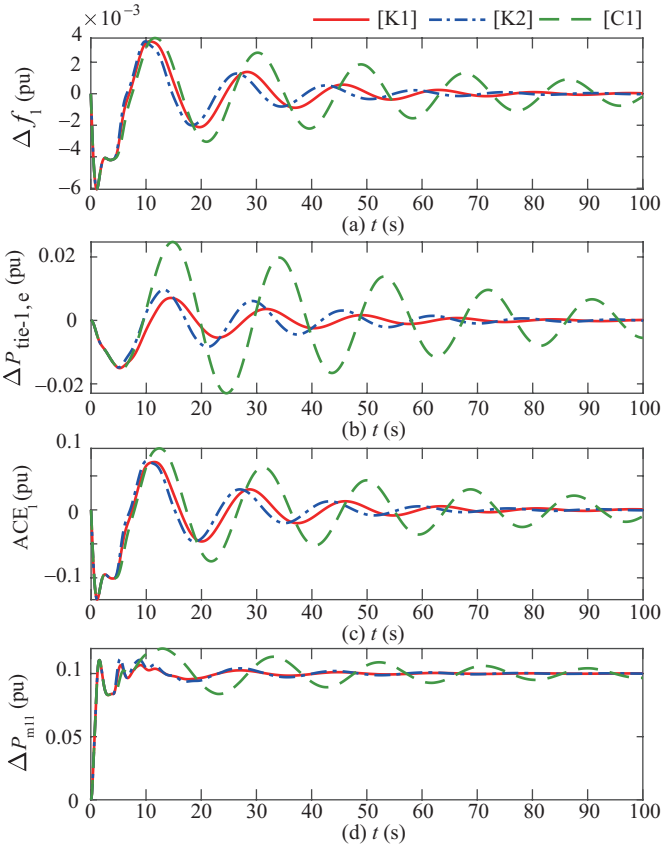

Figure 8: Comparisons of responses for area 1 in three-area LFC scheme with constant delays and step loads

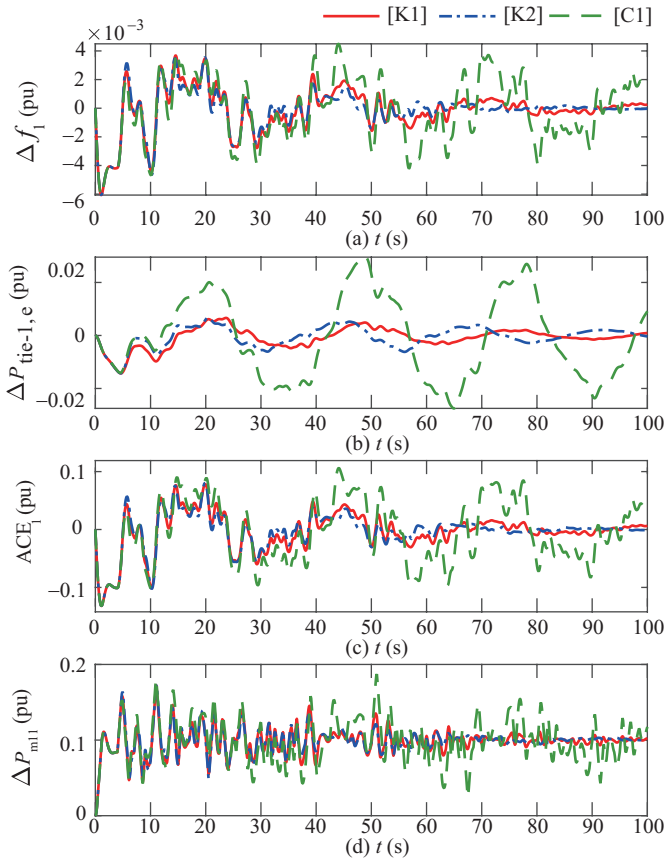

Figure 9: Comparisons of responses for area 1 in three-area LFC scheme with random delays and step loads

As can be seen, the performances of these two controllers are almost identical and both of them maintain the stability of the delayed LFC schemes effectively.

For scenario 3, the closed-loop system is tested under different parameter variations (PV), PV $\in [-30\%, 30\%]$ since the modeled dynamical systems, in practice, may experience sudden variations in their parameters or structures due to the failure of components, environmental disturbances, different operating conditions, etc. This simulation aims to check whether the two controllers obtained based on normal parameters have similar robustness against parameter variations.

The integral of the time multiplied absolute value of the error (ITAE), and the figure of demerit (FD) are defined as

$$ITAE = \int_0^{100} t\,(|ACE_1| + |ACE_2| + |ACE_3|)\,dt \tag{21}$$

$$FD = \sum_{i=1}^{3} \left[(OS_i \times 10)^2 + (FU_i \times 4)^2 + (Ts_i \times 0.3)^2\right] \tag{22}$$

where OS_i, FU_i and Ts_i represent the overshoot, first undershoot, and settling time of the frequency deviation in area i, respectively. Therefore, considering the cases i.e., $h_a = 4$s, $h_b \in$ [0s, 10s], the results are shown in Table 6.

From Table 6, we can find even though the degree of PV is up to ±30%, both controllers K_1 and K_2 are capable of eliminating the frequency deviations when different cases of time delays are taken into account. Their robustness against PV is thus

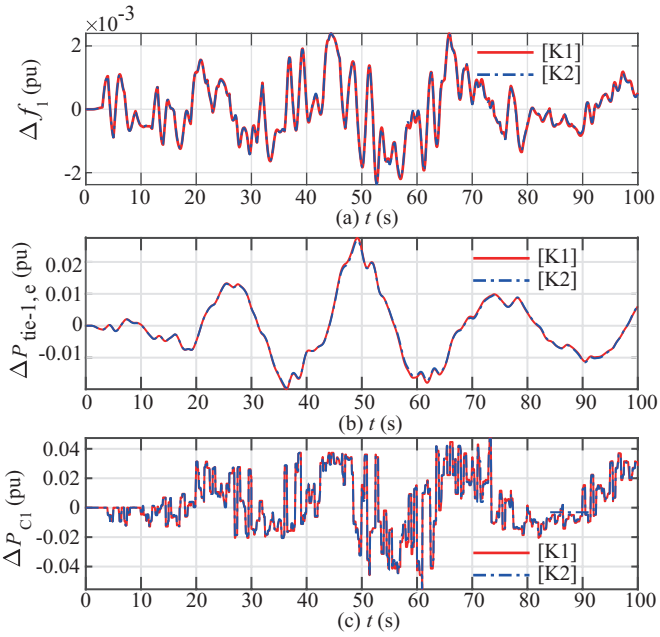

Figure 10: Comparisons of responses for area 1 in three-area LFC scheme with random delays and random loads

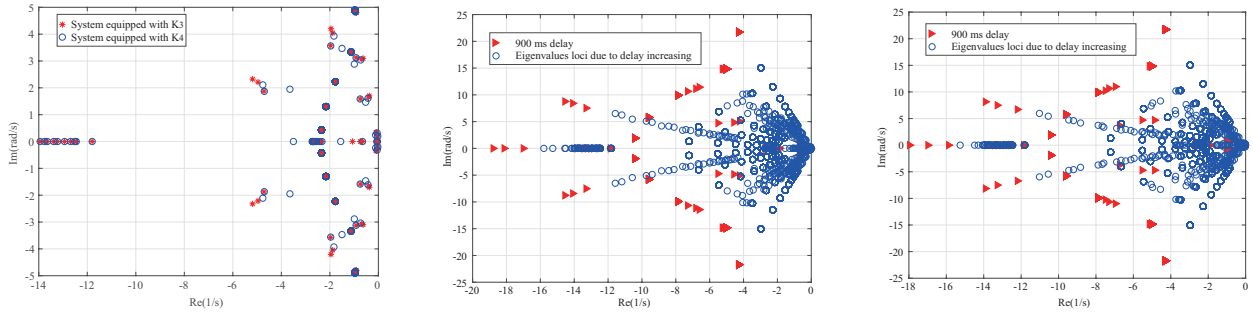

(i) (ii) (iii)

Figure 11: (i) Eigenvalues of NE39 system equipped with K_3 or K_4. (ii) Eigenvalues loci of NE39 system equipped with K_3 as delay increases. (iii) Eigenvalues loci of NE39 system equipped with K_4 as delay increases.

Table 6: Comparisons of performance indices including ITAE and FD

	ITAE (h_a)		FD (h_a)		ITAE (h_b)		FD (h_b)	
PV (%)	K_1	K_2	K_1	K_2	K_1	K_2	K_1	K_2
-30	40	31	116	103	65	48	243	170
-20	46	35	123	110	55	36	128	98
-10	55	41	132	119	57	36	130	60
0	67	50	196	128	66	44	179	86
10	83	63	258	209	79	55	216	148
20	105	81	329	230	93	68	221	187
30	138	107	463	355	111	85	372	196

demonstrated. Moreover, the ITAE and the FD obtained from the LFC scheme equipped with K_1 are larger than that from the system controlled by K_2. That is, based on the original model, controller K_2 can address the PV better in comparison with controller K_1 developed from the proposed model. Whereas, in Section 4.1, we have verified that the cost of computing K_1 is significantly reduced. The little sacrifice of dynamic performance to computation efficiency is allowable and acceptable.

4.3. Validation on NE39 System

1) Controller Design: The 10-unit NE39 system is divided into three areas, i.e., for area 1 and 3, each area contains 3 units, and for area 2, 4 units are included. Hence, we have $N = 3$ and $n_1 = 3, n_2 = 3, n_3 = 4$. The transformation matrix E_{T2} employed for obtaining the CTODE model is given in below.

$$
\begin{aligned}
E_{\mathrm{T2}} &= [E_{3\mathrm{a}}, E_{3\mathrm{b}}, E_{3\mathrm{c}}]^T \\
E_{3\mathrm{a}} &= [E_1, E_2, E_9, E_{10}, E_{11}, E_{18}, E_{19}, E_{28}] \\
E_{3\mathrm{b}} &= [E_3, \ldots, E_5, E_{12}, \ldots, E_{14}, E_{20}, \ldots, E_{23}] \\
E_{3\mathrm{c}} &= [E_6, \ldots, E_8, E_{15}, \ldots, E_{17}, \ldots, E_{24}, \ldots, E_{27}] \\
E_l &= [0_{1\times(l-1)}, 1, 0_{1\times(28-l)}]^T, l = 1, 2, \ldots, 28.
\end{aligned}
$$

The typical parameters for turbines, governors, and droop characteristic are $T_g = 0.08s$, $T_t = 0.40s$, and $R = 0.05$, respectively. For the numerical test, the actual values for T_g , T_t, and R are randomly generated in the range of $[1 \pm 10\%]$ of the typical values given above.

This case study investigates the controller design considering random delays. Provided that the upper bounds of the random delays are given as 2s, i.e., $h_{\mathrm{given}} = 2$ in Theorem 1 while setting weight matrix $Q_1 = 0$. Thus, Theorem 1 shows the relationship between γ and the PI gains. To minimize the influence of time delays, load disturbances, and parameter variations on the system frequency, the controller gains are optimized by the PSO algorithm again. The results of controllers with respect to the RPI are shown in Table 5, where K_3 and K_4 are designed based on the CTODE model and original model, respectively. As we can see, the corresponding RPI for K_3 is 7.51, which approximates the value of RPI for K_4. Thus, the dynamic performances of K_3 and K_4 are expected to be similar.

2) System Eigenvalue Analysis: Similarly, the Chebyshev discretization method is to analyze the eigenvalues of the NE39 system equipped with controllers K_3 or K_4. When the upper bound of time delay is set to 4 s for analyzing the NE 39 system, its eigenvalues are described as shown in Figure 11(i). From Figure 11(i), both controllers K_3 and K_4 enable the NE 39 system to be stable, although they are designed by considering the time delays equal to 2 s. Additionally, the eigenvalues for two NE 39 systems equipped with different controllers are located closely. Hence, comparing with K_4 based on the original model, the robustness against time delays of K_3 using the CTODE model is verified to be almost unchanged theoretically.

Then, assume the upper bounds of random delay increase from 900 ms to 4.5 s by the step of 400 ms. The eigenvalues loci are characterized in Figure 11(ii) and 11(iii), where Figure 11(ii) describes the NE 39 system controlled by K_3, and Figure 11(iii) shows the NE 39 system with controller K_4. Due to the increased time delays, the eigenvalues loci in both Figure 11(ii) and 11(iii), tend to move toward the right side but never go through the imaginary axis. Moreover, the similar eigenvalues loci can be observed from Figure 11(ii) and 11(iii). Thus, as time delays are increased, the similar dynamic performance of controllers K_3 and K_4 is validated.

3) Simulation Verification: The NE39 system is employed to further verify the similar dynamic characteristics of controllers K_3 and K_4 that are obtained based on the CTODE model and the original model, respectively. Thus, the availability of the

proposed CTODE model for designing controllers in the actual power system, can be verified. For simulations, the generator parameters for 10 unit NE39 system refer to [35]. Two scenarios are provided.

For scenario 4, the time delays are given as constants equal to 4 s in simulation. The step fluctuations are assumed to the NE39 system, i.e., ΔP_{d1} =0.1 pu, ΔP_{d2} = 0.08 pu, and ΔP_{d3} =0.05 pu. The system responses are recorded in Figure 12. It is clear that after the step loads are given, the variations of ACE_1 and Δf_1 controlled by K_3 or K_4 are approaching each other.

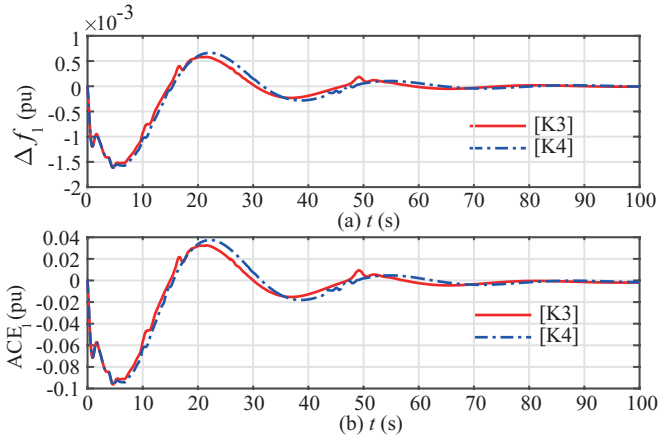

Figure 12: Comparisons of responses for area 1 in the 10-unit NE39 system with constant delays and step loads controlled by different controllers

For scenario 5, the random delays and loads are applied to the NE39 system, for which we have $\tau(t) \in [0, 10]$ s and $\Delta P_{\mathrm{di}} \in [-0.02, 0.02]$ pu, $i = 1, 2, 3$. For simulation, these random delays and loads are described in Figure 7 similarly. From Figure 13, it can be found that the dynamic tendencies of ACE_1 suppressed by K_3 or K_4, are almost identical. Same observations can be obtained for the variations of states $\Delta P_{tie-1,e}$ and ΔP_{C1}. Therefore, the method proposed in this paper, is verified to be effective in designing controllers for the real-world system while guaranteeing their robust dynamic performances.

5. Conclusion

This paper has investigated an effective method to improve the efficiency of tuning the robust controller in the large load frequency control (LFC) scheme considering time delay. A novel constraint time-delayed ordinary differential equation (CTODE) model has been proposed, for which the way of each state participating into the LFC model has been observed carefully. Compared with the original model, the CTODE model is an equivalent form, including a delayed part, a delay-free part, and a delay-related part. Since the remote signals influenced by communication delays are contained in the delayed part, its order is small and keeps unchanged with the increased scale of the system. Then, based on the CTODE model, a new Lyapunov functional has been constructed by introducing the delayed part to deal with the time delays. Thus, based on the H_∞ performance analysis, a new bounded real lemma (BRL) has been developed with enhanced efficiency.

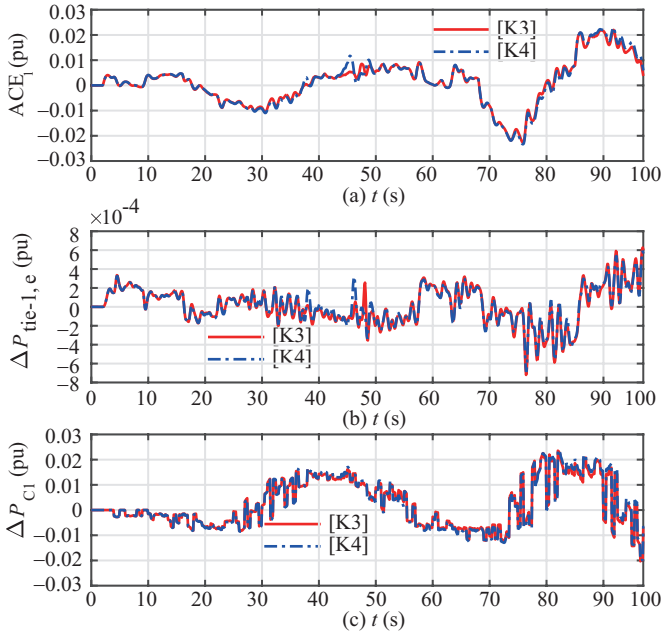

Figure 13: Comparisons of responses for area 1 in the 10-unit NE39 system with random delays and loads controlled by different controllers

Case studies have been carried out on the three-area LFC schemes and 39 bus New England systems. The obtained criterion has been shown with significantly improved calculation efficiency in large power systems. It has been verified that the obtained criterion is applicable for the delay-dependent stability analysis of large-scale power systems with the cost of little computation accuracy. Most importantly, this criterion has been validated for guiding the design of robust controllers in large power systems efficiently without sacrificing the dynamic performances of the designed controllers. The comparisons have been made between the controllers designed with the CTODE model and the original model in terms of robustness against time delays, load variations, and parameter uncertainties.

In the smart grid, the plug-in electric vehicles (PEVs) can provide the additional primary frequency control by adding the PEVs control loop into the traditional power system. The charging/discharging power of PEVs depends on the vehicle-to-grid schemes, and the frequency deviation is the input signal. The transmission delays of the remote signal occur. Thus, the proposed method is applicable for investigating the frequency regulation in multi-area power systems with PEVs. Moreover, as wide-area damping control systems (WADCs) employ a few remote information as inputs by using the transmission channels, the presented method can be used to study the delay-dependent stability analysis and controller design for the WADCs efficiently.

In addition, this paper investigates the LFC problem based on the linearised model around one operation point, which is valid for the LFC of the traditional power system. For this system, the real power is delivered by a synchronous generator and controlled by the mechanical power output of a steam turbine, hydro-turbine etc., to match the time-varying load demand. For a future power system with high-penetration level

of intermittent renewable energy generation, increased flexible load, and operation in an electricity market environment, its operating point tends to vary more frequently and not around one nominal operation point as the conventional power system. Under those new cases, the frequency control of the future power system demands to consider all those nonlinear dynamics with a nonlinear power system model, including the generation rate constraints and the governor dead band, etc. Thus, the frequency stability analysis and control should be carried out based on the nonlinear power systems model, which will be our future work.

Appendix I

The following table lists the parameters of the three-area LFC scheme.

Table 7: Parameters of three-area LFC system with three generators

	T_t	T_g	R	D	β	M	T_{ij}
Area1	0.3	0.1	0.05	1	21	10	$T_{12}=0.1968, T_{13}=0.2148$
Area2	0.4	0.17	0.05	1.5	21.5	12	$T_{21}=0.1968, T_{23}=0.1830$
Area3	0.35	0.2	0.05	1.8	21.8	12	$T_{31}=0.2148, T_{32}=0.1830$

Appendix II

The detailed proof of Theorem 1 is presented in this part.

The Wirtinger-based inequality is recalled in the following lemma to bound the derivative of the Lyapunov functional.

Lemma 1. *[33, 34] For a given matrix $Z > 0$, the following inequality holds for all continuously differentiable functions x in $[a, b] \longrightarrow R^m$:*

$$(b-a)\int_a^b \dot{x}^T(s)Z\dot{x}(s)ds \geq \tilde{\Omega}_1^T Z\tilde{\Omega}_1 + 3\tilde{\Omega}_2^T Z\tilde{\Omega}_2 \tag{23}$$

where $\tilde{\Omega}_1 = x(b) - x(a)$ and $\tilde{\Omega}_2 = x(b) + x(a) - \frac{2}{b-a}\int_a^b x(s)ds$

Proof: Calculating the derivative of (10) along system (8) yields

$$\begin{aligned}\dot{V}(t) = {} & 2\xi^T(t)P\dot{\xi}(t) + x_1^T(t)(Q_1+Q_2)x_1(t) \\ & - (1-\dot{\tau}(t))x_1^T(t-\tau(t))Q_1x_1(t-\tau(t)) - x_1^T(t-h)Q_2x_1(t-h) \\ & + h^2\dot{x}_1^T(t)R\dot{x}_1(t) - h\int_{t-h}^t \dot{x}_1^T(s)R\dot{x}_1(s)ds\end{aligned}$$

where $\dot{\xi}^T(t) = \left[\dot{x}_1^T(t), \dot{x}_2^T(t), \dot{x}_3^T(t), x_1^T(t) - x_1^T(t-h)\right]$.
$\dot{V}(t)$ can be rewritten in below.

$$\begin{aligned}\dot{V}(t) = {} & \varsigma^T(t)\Big(E_a^TPE_b + E_b^TPE_a + e_1^T(Q_1+Q_2)e_1 \\ & - (1-\dot{\tau}(t))e_2^TQ_1e_2 - e_3^TQ_2e_3 + h^2e_{s1}^TRe_{s1}\Big)\varsigma(t) \\ & - h\int_{t-h}^t \dot{x}_1^T(s)R\dot{x}_1(s)ds\end{aligned} \tag{24}$$

with $\varsigma^T(t) = \left[x_1^T(t), x_1^T(t-\tau(t)), x_1^T(t-h), \frac{1}{h}\int_{t-h}^t x_1^T(s)ds, x_2^T(t), x_3^T(t), \omega^T(t)\right]$, and other matrices are defined in (11).

Thus, by using inequality (23) to estimate the integral term in (24), we have

$$\begin{aligned}-h\int_{t-h}^t \dot{x}_1^T(s)R\dot{x}_1(s)ds \leq & -\left[\Omega_1^T\ \Omega_2^T\right]\mathrm{diag}\{R, 3R\}\left[\Omega_1^T\ \Omega_2^T\right]^T \\ \leq & -\varsigma^T(t)E_c^T\,\mathrm{diag}\{R, 3R\}\,E_c\varsigma(t)\end{aligned} \tag{25}$$

where $\Omega_1 = x(t) - x(t-h)$ and $\Omega_2 = x(t) + x(t-h) - \frac{2}{h}\int_{t-h}^t x(s)ds$, and E_c is shown as (11).

When the time-varying delay satisfies $0 \leq \tau(t) \leq h$ and $\dot{\tau}(t) \leq \mu$, we obtain the following inequality by combining the results in (24) and (25):

$$\dot{V}(t) \leq \varsigma^T(t)\Pi_1\varsigma(t) \tag{26}$$

where Π_1 is defined in (11).

Meanwhile, using Π_2 given in (11), we have $\varsigma^T(t)\Pi_2\varsigma(t) - y^T(t)y(t) + \gamma^2\omega^T(t)\omega(t) = 0$.

It is obvious that

$$\dot{V}(t) \leq \varsigma^T(t)(\Pi_1+\Pi_2)\varsigma(t) - y^T(t)y(t) + \gamma^2\omega^T(t)\omega(t) \tag{27}$$

Therefore, one can see if inequality (11) holds, then

$$\dot{V}(t) \leq -y^T(t)y(t) + \gamma^2\omega^T(t)\omega(t) \tag{28}$$

Under the initial condition that $V(0) = 0$, the integration of both sides in (28) from 0 to $+\infty$ leads to

$$V(+\infty) \leq \int_0^{+\infty}\left[-y^T(t)y(t) + \gamma^2\omega^T(t)\omega(t)\right]dt \tag{29}$$

Hence,

$$\int_0^{+\infty} y^T(t)y(t)dt \leq \int_0^{+\infty}\gamma^2\omega^T(t)\omega(t)dt \tag{30}$$

and $\|y(t)\| \leq \gamma\|\omega(t)\|$ exists for any nonzero $\omega(t) \in \mathcal{L}_2[0, +\infty)$. Moreover, when considering the condition that $\omega(t) = 0$, based on inequality (28), we obtain $\dot{V}(t) \leq -\varepsilon\|x(t)\|^2$ for a sufficient small scalar $\varepsilon > 0$ and $x(t) \neq 0$. As a result, the asymptotical stability of system (8) is guaranteed.

6. References

[1] P. Kundur. "*Power System Stability and Control*," New York: McGraw-Hill, 1994.

[2] X.C. Shangguan, Y. He, C.K. Zhang, et al. "Switching system-based load frequency control for multi-area power system resilient to denial-of-service attacks," *Control Eng. Pract.,* vol. 107, pp. 104678, 2020.

[3] S. Bhowmik, K. Tomsovic, A. Bose, "Communication models for third party load frequency control," *IEEE Trans. Power Syst.,* vol. 19, no. 1, pp. 543-548, 2004.

[4] C. Peng, J. Zhang, H. Yan, "Adaptive event-triggering H_∞ load frequency control for network-based power systems," *IEEE Trans. Ind. Electron.,* vol. 65, no. 2, pp. 1685-1694, 2018.

[5] L. Jin, Y. He, C.K. Zhang, et al. "Equivalent input disturbancebased load frequency control for smart grid with air conditioning loads," *Sci. China Inf. Sci.,* DOI: 10.1007/s11432-020-3120-0, 2020.

[6] H. Bevrani. *"Robust Power System Frequency Control,"* New York: Springer, 2009.

[7] X.C. Shangguan, Y. He, C.K. Zhang, et al. "Robust load frequency control for power system considering transmission delay and sampling period," *IEEE Trans. Industr. Inform.,* vol. 17, no. 8, pp. 5292-5303, 2021.

[8] L. Jiang, W. Yao, Q.H. Wu, et al. "Delay-dependent stability for load frequency control with constant and time-varying delays," *IEEE Trans. Power Syst.,* vol. 27, no. 2, pp. 932-941, 2012.
[9] S. Sonmez, S. Ayasun, C.O. Nwankpa, "An exact method for computing delay margin for stability of load frequency control systems with constant communication delays," *IEEE Trans. Power Syst.,* vol. 31, no. 1, pp. 1-8, 2016.
[10] C.K. Zhang, L. Jiang, Q.H. Wu, et al. "Further results on delay-dependent stability of multi-area load frequency control," *IEEE Trans. Power Syst.,* vol. 28, no. 4, pp. 4465-4474, 2013.
[11] F. Yang, J. He, D. Wang, "New stability criteria of delayed load frequency control systems via infinite-series-based inequality," *IEEE Trans. Ind. Inf.,* vol. 14, no. 1, pp. 231-240, 2018.
[12] F. Yang, J. He, Q. Pan, "Further improvement on delay-dependent load frequency control of power systems via truncated B-L inequality," *IEEE Trans. Power Syst.,* vol.33, no. 5, pp. 5062-5071, 2018.
[13] C. Peng, J. Li, M. Fei, "Resilient event-triggering H_∞ load frequency control for multi-area power systems with energy-limited DoS attacks," *IEEE Trans. Power Syst.,* vol. 32. no. 5, pp. 4110-4118, 2017.
[14] C. Peng, J. Zhang, "Delay-distribution-dependent load frequency control of power systems with probabilistic interval delays," *IEEE Trans. Power Syst.,* vol. 31, no. 4, pp. 3309-3317, 2016.
[15] C.K. Zhang, L. Jiang, Q.H. Wu, et al. "Delay-dependent robust load frequency control for time delay power systems," *IEEE Trans. Power Syst.,* vol. 28, no. 3, pp. 2192-2201, 2013.
[16] C. Duan, C.K. Zhang, L. Jiang, et al. "Structure-exploiting delay-dependent stability analysis applied to power system load frequency control," *IEEE Trans. Power Syst.,*, vol. 32, no. 6, pp. 4528-4540, 2017.
[17] X.D. Yu, H.J. Jia, C.S. Wang, "CTDAE and CTODE models and their applications to power system stability analysis with time delays," *Sci. China Tech. Sci.,* vol. 56, no. 5, pp. 1213-1223, 2013.
[18] L. Jin, C.K. Zhang, Y. He, et al. "Delay-dependent stability analysis of multi-area load frequency control with enhanced accuracy and computation efficiency," *IEEE Trans. Power Syst.,* vol. 34, no. 5, pp. 3687-3696, 2019.
[19] L. Jin, Y. He, C.K. Zhang, et al. "Robust delay-dependent load frequency control of wind power system based on a novel reconstructed model," *IEEE Trans. Cybern.,* 2021, DOI: 10.1109/TCYB.2021.3051160.
[20] W. Yao, L. Jiang, Q. Wu, et al. "Delay-dependent stability analysis of the power system with a wide-area damping controller embedded," *IEEE Trans. Power Syst.,* vol. 26, no. 1, pp. 233-240, 2011.
[21] W. Yao, L. Jiang, J. Wen, et al. "Wide-area damping controller of facts devices for inter-area oscillations considering communication time delays," *IEEE Trans. Power Syst.,* vol. 29, no. 1, pp. 318-329, 2014.
[22] F. Ma, V. Vittal, "A hybrid dynamic equivalent using ANN-based boundary matching technique," *IEEE Trans. Power Syst.,* vol. 27, no. 3, pp. 1494-1502, 2012.
[23] M.H. Rezaeian, S. Esmaeili, R. Fadaeinedjad, "Generator coherency and network partitioning for dynamic equivalencing using subtractive clustering algorithm," *IEEE Syst. J.,* vol. 12, no. 4, pp. 3085-3095, 2018.
[24] J.J. Sanchez-Gasca, J.H. Chow, "Power system reduction to simplify the design of damping controllers for interarea oscillations," *IEEE Trans. Power Syst.,* vol. 11, no. 3, pp. 1342-1349, 1996.
[25] S. Ghosh, N. Senroy, "Balanced truncation based reduced order modeling of wind farm," *Int. J. Elect. Power Energy Syst.,* vol. 53, pp. 649-655, 2013.
[26] S. Ghosh, Y.J. Isbeih, M.S. El Moursi, et al. "Cross-Gramian model reduction approach for tuning power system stabilizers in large power networks," *IEEE Trans. Power Syst.,* vol. 35, no. 3, pp. 1911-1922, 2020.
[27] C. Li, Z. Du, Y. Ni, et al. "Reduced model-based coordinated design of decentralized power system controllers," *IEEE Trans. Power Syst.,* vol. 31, no. 3, pp. 2172-2181, 2016.
[28] Y. Ni, Z. Du, C. Li, et al. "Cross-Gramian-based dynamic equivalence of wind farms," *IET Gener., Transmiss. Distrib.,* vol. 10, no. 6, pp. 1422-1430, 2016.
[29] H. Fan, L. Jiang, C.K. Zhang, et al. "Frequency regulation of multi-area power systems with plug-in electric vehicles considering communication delays," *IET Gener. Transm. Distrib.,* vol. 10, no. 14, pp. 3481-3491, 2016.
[30] X. Liu, Y. Zhang, K.Y. Lee, "Robust distributed MPC for load frequency control of uncertain power systems," *Control Eng. Pract.,* vol. 56, pp. 23-47, 2016.
[31] F. Milano, "Small-Signal stability analysis of large power systems with inclusion of multiple delays," *IEEE Trans. Power Syst.,* vol.31, no. 4, pp. 3257-3266, 2016.
[32] C. Li, J. Wu, C. Duan, et al. "Development of an effective model for computing rightmost eigenvalues of power systems with inclusion of time delays," *IEEE Trans. Power Syst.,* vol. 34, no. 6, pp. 4216-4227, 2019.
[33] A. Seuret, F. Gouaisbaut, "Wirtinger-based integral inequality: Application to time-delay systems," *Automatica*, vol. 49, pp. 2860-2866, 2013.
[34] C.K. Zhang, Y. He, L. Jiang, et al. "Stability analysis of systems with time-varying delay via relaxed integral inequalities," *Syst. Control. Lett.,* vol. 92, pp. 52-61, 2016.
[35] T. Athay, R. Podmore, S. Virmani, "A practical method for the direct analysis of transient stability," *IEEE Trans. Power App. Syst.,* vol. PAS-98, no. 2, pp. 573-584, 1979.